THE MEASUREMENT OF AERODYNAMIC FORCES AND MOMENTS IN THE NOL 4-IN. HYPERSONIC SHOCK TUNNEL NO. 3

7 SEPTEMBER 1961

NOL

UNITED STATES NAVAL ORDNANCE LABORATORY, WHITE OAK, MARYLAND

Ballistics Research Report 51

THE MEASUREMENT OF AERODYNAMIC FORCES AND MOMENTS IN THE NOL 4-IN. HYPERSONIC SHOCK TUNNEL NO. 3

Prepared by:

D. F. Gates and D. N. Bixler

ABSTRACT: Two light-weight models of missiles are suspended by very fine threads in the test section of the NOL 4-in. Hypersonic Shock Tunnel No. 3. Alongside the models, a light-weight sphere is suspended. A high-speed camera is focused on the models through a window in the side of the shock tunnel receiver tank and illumination of the models is provided by a short-duration, high-intensity light source. When the shock tunnel is fired, the light source is actuated, the fine threads holding the models are snapped, and the models are then photographed for 2-1/4 milliseconds as they move freely in the shock tunnel flow. From the high-speed camera film (taken at a frequency of about one frame every 40 microseconds) data of the horizontal, vertical, and angular motions of the models as functions of time are obtained. Data of the motion of the sphere are also obtained. Since the aerodynamic characteristics of a sphere are fairly well established, this configuration is employed as a calibration body, and the motions of the models are compared to that of the sphere. By various methods of comparison the aerodynamic drag, lift, and moment coefficients of the models are determined.

PUBLISHED NOVEMBER 1961

U. S. NAVAL ORDNANCE LABORATORY
White Oak, Silver Spring, Maryland

This work was sponsored by the Re-Entry Body Section of the Special Projects Office, Bureau of Naval Weapons, under the Applied Research Program in Aeroballistics.

This report supersedes NavOrd Report 6843, to be withheld from publication.

W. D. COLEMAN
Captain, USN
Commander

A. E. SEIGEL
By direction

Table of Contents

Illustrations

LIST OF SYMBOLS

C_M	aerodynamic moment coefficient of model
C_L	aerodynamic lift coefficient of model
C_D	aerodynamic drag coefficient of model
C_{D_s}	aerodynamic drag coefficient of sphere
x	coordinate of center of gravity of model (increasing in direction of flow)
y	coordinate of center of gravity of model (increasing in direction normal to flow)
x_2	coordinate of any point, other than center of gravity, on centerline of model (increasing in direction of flow)
y_2	coordinate of any point, other than center of gravity, on centerline of model (increasing in direction normal to flow)
x_s	coordinate of center of gravity of sphere (increasing in direction of flow)
y_s	coordinate of center of gravity of sphere (increasing in direction normal to flow)
α	angle of attack of model (= arc tan $-\frac{y-y_s}{x-x_s}$)
t	time
ω	first derivative of α with respect to time
$\ddot{x}$	second derivative of x with respect to time
$\ddot{y}$	second derivative of y with respect to time
$\ddot{\alpha}$	second derivative of α with respect to time
$\ddot{x}_s$	second derivative of x_s with respect to time
$\overline{\alpha}$	average value of α over an interval of time
$\overline{\lvert\alpha\rvert}$	average value of the absolute value of α over an interval of time
x_1	initial value of x, when t=o; also experimental value of x at time t_1

y_i	initial value of y, when t=0; also experimental value of y at time t_i
x_{si}	initial value of x_s, when t=0; also experimental value of x_s at time t_i
α_i	initial value of α, when t=0; also experimental value of α at time t_i
m	mass of model
m_s	mass of sphere
I	moment of inertia of model about its center of gravity
D_m	characteristic diameter of model
A_m	characteristic area of model
A_s	characteristic area of sphere
ρ	density of flow in test section
u	velocity of flow with respect to test section
u_s	velocity of sphere with respect to test section
u_m	velocity of model with respect to test section
q	dynamic pressure of flow with respect to test section ($=1/2\,\rho\,u^2$)
q_s	dynamic pressure experienced by sphere ($=1/2\,\rho\,(u-u_s)^2$)
q_m	dynamic pressure experienced by model ($=1/2\,\rho\,(u-u_m)^2$)
M	Mach number of flow
R_e	Reynolds number of flow
P_m	free-stream pressure behind shockwave at muzzle
X	distance from muzzle diaphragm along centerline of flow to model
Y	normal distance from centerline of flow to model
Y_s	normal distance from centerline of flow to sphere

THE MEASUREMENT OF AERODYNAMIC FORCES AND MOMENTS IN THE NOL 4-IN. HYPERSONIC SHOCK TUNNEL NO. 3

INTRODUCTION

1. In order to create conditions in the laboratory similar to the conditions encountered by a high-speed missile in a re-entry trajectory at an altitude of 50,000 to 100,000 feet, the Naval Ordnance Laboratory constructed the NOL 4-In. Hypersonic Shock Tunnel No. 3. On 3 September 1958, the first experiment with this facility was performed. Since then, most of the tests in this shock tunnel have been made for the purpose of determining the static aerodynamic drag, lift, and moment coefficients of models of missiles as functions of missile angle of attack and Mach number. In each test, this was accomplished by observing the motion of light-weight models in the test section while these models were in actual free flight in the shock tunnel flow. The experimental technique followed in each test was first briefly described by representatives of the Naval Ordnance Laboratory at the Second Shock Tube Symposium in 1958 (reference (a)). A more elaborate description was given in April 1959 (reference (b)) and in May 1959 (reference (c)). The technique, with several modifications, is also being used by the Missile and Space Vehicle Department of the General Electric Company in its 6-in. shock tunnel (reference (d)). Since the first test was made in 1958, different experimental procedures and methods of data analysis have been employed. All of the various experimental and analytical methods are described below.

EXPERIMENTAL TECHNIQUE

2. Figure 1 is an illustration of the NOL 4-in. Hypersonic Shock Tunnel No. 3.* Figures 2 and 3 give some of the dimensions of the various parts of the shock tunnel. The high-pressure chamber (which subsequently will be referred to as the "chamber") is 12 feet long and has an inside diameter of 10 inches. The low-pressure chamber (which will be referred to as the "barrel") is 60 feet long and has an inside diameter of 4 inches, while the receiver tank is 54 feet long and 8 feet in diameter. Between the chamber and the barrel is a flat stainless-steel diaphragm which has a thickness of about 0.3 inches. A piston is placed next to the diaphragm, though in many tests the

---

* A general description of this facility and its instrumentation can be found in reference (e).

piston is excluded. It is made of nylon or aluminum and weighs from 200 to 550 grams. Several pressure gages* are mounted through holes at various stations along the side of the barrel, so that the pressure P_m of the air at these stations can be monitored. At the receiver tank the barrel diameter increases conically from 4 inches to 10 inches. This increase takes place over a distance of 9.6 inches, and at a distance of 6.4 inches from the large end of the increase there is a hemispherical steel diaphragm 6 inches in diameter and tapered in thickness from 0.12 inch at the center to 0.30 inch at the perimeter. This muzzle arrangement serves to prevent disturbances from the opening hemispherical diaphragm from interfering with the flow over the models by allowing these disturbances to diverge as they enter the test section.

3. The flow is allowed to expand in a free jet from the muzzle into the receiver tank. Thus, the flow over the models in the test section is radial, and the test section Mach number increases with increasing distance from the muzzle. At various distances from the muzzle, pairs of opposing windows are located in the sides of the receiver tank, as shown in Figure 3, so that models may be placed between any pair of windows, depending upon the flow conditions desired.** The distances between the muzzle and the windows shown in Figure 3 may be conveniently changed by adding a 3-foot extension to the barrel. Also, the most distant three windows are all mounted on a plate which can be shifted downstream by one foot. Models are most commonly tested at distances to 80, 128, or 218 inches from the muzzle. Table I lists the standard loading conditions and approximate flow conditions observed when testing at these positions in the test section. The flow duration is approximately 2-1/4 milliseconds, except for the Mach 14.3 case, where it is slightly less than 2 milliseconds. In all cases shown in this table, the chamber is loaded with 6,000 psi of helium, and the helium is heated by burning 30 lbs. of Hercules Unique powder. The powder is ignited

---

* A detailed description of the type of gages used in this shock tunnel is given in references (f) and (g).

**Tests have shown that between any pair of windows the axial gradient of the Mach number over a distance of 4 inches is always less than 2-1/2 percent of the Mach number, while calculations have revealed that radial gradients in Mach number over a distance of 6 inches off the centerline of flow are always less than 2-1/2 percent of the Mach number (cf., reference (h)).

by a series of explosive primers running the length of the chamber. In some instances the chamber is loaded with a mixture of oxygen, hydrogen, and helium, in a 1/3/8 molar proportion, respectively, instead of helium and powder. This mixture is also ignited by the same arrangement of explosive primers. Though the helium powder mixture produces a less efficient driver, it is more commonly used because there is little chance of an undesirable detonation occurring during ignition of the powder. At the same time efficiency is not the object, but high densitites and long flow durations are more desirable.

4. In the test section, two light-weight models and a light-weight sphere are suspended by very fine threads. Figure 4 is a photograph of two models, (in this case, hollow cones) and a sphere suspended by threads. This is a view from the rear of the receiver tank looking forward into the muzzle. Outside one window a short-duration, high-intensity light source is situated so as to pass a converging beam of light through the receiver tank and over the models.* A system of several horizontal and vertical grid wires is attached to the window nearest the light source. This system of wires serves as a reference system, and can be removed from one window and placed on any other window. A Beckman & Whitley Dynafax high-speed framing camera is placed on the opposite side of the receiver tank and focused on the models. This camera is capable of taking pictures at a rate as high as one frame per 40 microseconds. In tests where a greater framing rate is desired, the Beckman & Whitley 192 model high-speed framing camera is used; however, inherent in this camera is a time-varying optical distortion (cf., reference (j)). The Dynafax model also has a minor amount of distortion, but it is essentially constant with time.

5. The models suspended in the test section weigh between one and 30 grams, and are from one to 6 inches long. They can be manufactured either by machining or by molding. If they are machined, they are usually made of ethocel, althougn various materials are sometimes used for different parts of a model. A portion may be made of magnesium, aluminum, brass, or steel, in order to increase strength of a particular part of a model or to position the center of gravity at a desired point. The tolerance on the machining is either $\pm$ 0.002 inch or $\pm$ 0.005 inch, depending upon the material machined. When a model is

---

* A detailed description of the light source is given in reference (i).

of such a design that it cannot be machined inexpensively, while at the same time a sufficiently large quantity of models is required, a mold is built, and the models are then molded. In this case, they are manufactured from a foamed plastic, and the tolerance on each model is kept within $\pm$ 0.002 inch. The sphere that accompanies the models in the test section has a diameter of 0.25 to 1.5 inches, the latter being the diameter of a ping pong ball, which is sometimes used. Each sphere weighs from 0.3 to 5 grams and, except for the ping pong ball, is made of nylon.

6. With two models and a sphere suspended in the test section and the shock tunnel instrumentation prepared, the test section is sealed off and evacuated to less than 30 microns pressure. The chamber is loaded with 30 lbs. of powder, the primer rod is inserted, and the breech is secured. The barrel is loaded with the desired pressure of air, while the chamber is loaded with helium. The camera is then started, and when the camera drum attains a rate of rotation of about 1,560 rps, the camera shutter is opened, and the primers are electrically detonated, igniting the powder. The helium, due to the powder combustion, is raised to a high temperature and pressure, causing the stainless-steel diaphragm to rupture. The heated helium then drives against the air in the barrel, forming a shockwave which propagates through the air toward the muzzle, raising the temperature, pressure, and velocity of the air, until the shock-wave strikes the hemispherical diaphragm, bursting it and allowing the air to expand into the test section and pass over the models. The light source is actuated by a piezoelectric shockwave detector* in the muzzle, and the threads holding the models are swept away by the initial portion of the flow. The models, initially at rest, are then accelerated, and as they move, they are photographed by the high-speed camera. From the camera film, data of the movements of each model are recorded, and the aerodynamic coef-ficients of drag, lift, and moment of the models are reduced from the data.

DATA ANALYSIS

7. All methods of data analysis developed herein are derived on the assumption that dynamic forces and moments, as well as

---

* The shockwave detector is described in reference (k).

the force of gravity*, are negligible. Thus, it is assumed throughout that the magnitudes of the various components of acceleration of a model are directly proportional to the static aerodynamic moment, lift, and drag on the model. The drag force on a model is

$$C_D q_m A_m = m\ddot{x} \tag{1}$$

where C_D is the model's drag coefficient, q_m is its dynamic pressure, A_m its characteristic area, m its mass, and $\ddot{x}$ its acceleration in the direction of the flow. The lift on the model is

$$C_L q_m A_m = m\ddot{y} \tag{2}$$

where C_L is the lift coefficient of the model, and $\ddot{y}$ is its acceleration normal to the direction of flow and in a plane parallel to the plane of the camera film. The static aerodynamic moment on the model is

$$C_M q_m A_m D_m = I\ddot{\alpha} \tag{3}$$

where C_M is the static moment coefficient of the model, D_m is the characteristic diameter of the model, I is the moment of inertia about its center of gravity, and $\ddot{\alpha}$ is its angular acceleration. Similarly, for the sphere in the test section the drag is

$$C_{D_S} q_S A_S = m_S \ddot{x}_S \tag{4}$$

where C_{D_S} is the drag coefficient of the sphere, q_S is the dynamic pressure on the sphere, A_S is its cross-sectional area, m_S its mass, and $\ddot{x}_S$ its acceleration.

---

* The force of gravity on a model is so small in comparison to the aerodynamic forces that its effects are undetectable in the short duration in which observations are made.

8. By various manipulations of equations (1) through (4), values of C_D, C_L, and C_M are determined directly from the experimental data. Through equation (4) the dynamic pressure experienced by each model is determined. Since the loading pressure and temperature and final pressure P_M in the muzzle are known from direct measurements, the entropy of the air can be found by use of the equations of conservation of fluid mass, momentum, and energy, and the equation of state of air.* It is assumed that the expansion of the air from the muzzle is isentropic, so that a value for the entropy at any point in the test section is known. Then the Mach number and various other properties of the flow in the test section can be calculated by use of the same equations of fluid dynamics and the equation of state, once the dynamic pressure q is found. For this purpose, equation (4) is again used in conjunction with the experimental data to determine the dynamic pressure. In these applications of equation (4), two assumptions are made: (1) the dynamic pressure q_s on the sphere is equal to the dynamic pressure q_m on the model, and (2) the dynamic pressure q_s on the sphere is equal to the dynamic pressure q as experienced by an observer standing in the test section.

9. After a finite period of time from the beginning of flow, however, the models and the sphere will have attained individual velocities, so that each will experience a dynamic pressure slightly different from that experienced by the others, and all will experience a dynamic pressure different from that experienced by a stationary observer in the test section. To an observer standing in the test section, the dynamic pressure is $q=1/2\rho u^2$, where ρ and u are, respectively, the density and the velocity of the flow. From the standpoint of the sphere, $q_s=1/2\,\rho\,(u-u_s)^2$, where u_s is the velocity of the sphere. On the model, $q_m=1/2\rho\,(u-u_m)^2$, where u_m is the velocity of the model. Now, the difference in dynamic pressures as seen from the model and as seen from the sphere is

$$
\begin{aligned}
q_m - q_s &= \tfrac{1}{2}\rho(u-u_m)^2 - \tfrac{1}{2}\rho(u-u_s)^2 \\
&= \tfrac{1}{2}\rho\left[(u-u_m)^2 - (u-u_s)^2\right] \\
&= \tfrac{1}{2}\rho\left\{(u-u_m)^2 - \left[(u_m-u_s)+(u-u_m)\right]^2\right\} \\
&= \tfrac{1}{2}\rho\left[2(u_m-u_s)(u-u_m)+(u_m-u_s)^2\right] \qquad (5)
\end{aligned}
$$

*Values for the equation of state of air are taken from references (l) and (m).

The difference in dynamic pressures as seen from a point stationary in the test section and as seen from the sphere is

$$q - q_s = \tfrac{1}{2}\rho u^2 - \tfrac{1}{2}\rho(u-u_s)^2$$

$$= \tfrac{1}{2}\rho\left[u^2 - (u-u_s)^2\right]$$

$$= \tfrac{1}{2}\rho(2uu_s - u_s^2) \qquad (6)$$

The models or the sphere seldom reach a velocity greater than 2 percent of the flow velocity. In the most extreme case, the sphere attained a velocity u_s of 300 ft/sec, but since the velocity of the flow is 6,300 ft/sec or higher, u_s and u_m are still less than 5 percent of u. Thus, equations (5) and (6) can be simplified by dropping out certain second-degree terms in u_m and u_s. These equations then become

$$q_m - q_s \simeq -\rho(u_m - u_s)(u - u_m)$$

$$q - q_s \simeq \rho u u_s$$

The percent errors introduced in the quantities q_m and q by observing the dynamic pressure from the standpoint of the sphere are then

$$\frac{q_m - q_s}{q_m} 100\% \simeq \frac{-\rho(u_m - u_s)(u - u_m)}{\frac{1}{2}\rho(u-u_m)^2} 100\%$$

$$= 2\frac{u_m - u_s}{u - u_m} 100\% \qquad (7)$$

$$\frac{q - q_s}{q} 100\% \simeq \frac{\rho u u_s}{\frac{1}{2}\rho u^2} 100\%$$

$$= 2\frac{u_s}{u} 100\% \qquad (8)$$

In each individual test, the models and the sphere are so designed that the difference between the velocity of each model and that of the sphere (i.e., $u_m - u_s$) is less than one percent of $u - u_m$. Thus, according to equation (7), the maximum difference between q_s and q_m is less than 2 percent of q_m. Therefore, the first assumption, $q_m = q_s$, involves a negligible error. The second assumption is that $q = q_s$. Thus, according to equation (8),

the error resulting from this assumption is less than 10 percent of q, since u_s is always less than 5 percent of u. This assumption is made for the purpose of conveniently determining the Mach number of the flow, and, as pointed out in reference (b), a 10 percent error in determining the dynamic pressure q results in an error of less than 2 percent in Mach number. With the use of the above assumptions, the dynamic pressure can now be determined by analysis of the sphere motion as photographed by the camera.

10. Obtained from the camera is a strip of film containing 30 to 80 consecutive frames of silhouettes of the models and the sphere in motion. This film is placed in the projector of the Universal Telereadex,* and images of the silhouettes in one frame are magnified and cast on an opaque screen. A full-scale drawing or template of the image of each model is made on a sheet of vellum, with the centerline and center of gravity of the model also placed on each template. These templates are then superimposed upon the images of the silhouettes in each consecutive frame of the film, and with the read-out system of the Telereadex, the coordinates of the center of gravity and one other position on the centerline of each model are recorded on IBM cards. Also recorded in the same manner are the coordinates of the sphere in each frame. As was mentioned earlier, however, the images in each frame of the film are distorted to some degree by the optical system of the high-speed camera.

11. If the Beckman & Whitley 192 camera is used, then the film taken from the camera is 35-mm size. Due to an inherent property of the optical system of the camera, images in each frame of the film are distorted differently from those of any other frame. To compensate for this distortion, a map of a fine grid system in each frame of the film is superimposed on an undistorted cartesian coordinate system. Then when an arbitrary point in any given

---

* Model 29A, built by Telecomputing Corporation, consists of a projector which magnifies film-size images as much as 44-1/2 times and casts these images on a white opaque screen. On the screen are a pair of perpendicular cross-wires, which can be manipulated by an operator. Magnetic reading heads in the machine sense the movements of these cross-wires and convey this information to the Telecordex, which records and reads out the position of the intersection of the cross-wires. The magnetic reading heads sense a movement of the cross-wires of $\frac{1}{355}$ inch.

frame is observed in the cartesian coordinate system of the Universal Telereadex, the observed coordinates are replaced by the corresponding coordinates in the mapped distorted system, and the values of the latter coordinates are taken as the actual position of the point.

12. If the Beckman & Whitley Dynafax is used, the models are photographed on 16-mm frames, situated alternately on each edge of a strip of 35-mm film. Images in the frames on one edge of the film suffer a small amount of distortion, while images in the frames on the opposite edge suffer a different distortion. However, the distortion in the frames on each edge of the film is nearly constant with time. When data of the position of a model with respect to time are taken from the film, the data points appear alternately deflected, as a result of the alternate distortion. In order to reduce the effects of this distortion, every coordinate in each frame of the data is averaged with the corresponding coordinates in the adjacent frame. For example, if in frame number n the coordinates of the center of gravity of a model are x_n and y_n, and in frame number n + 1, the coordinates are x_{n+1}, and y_{n+1} then the final value given for the position of the model is

$$\left(\frac{x_n + x_{n+1}}{2}, \frac{y_n + y_{n+1}}{2}\right)$$

The data obtained from the film are thus reduced to the graphical form

$$\left.\begin{aligned} x &= x(t) \\ y &= y(t) \\ \alpha &= \alpha(t) \\ x_s &= x_s(t) \\ y_s &= y_s(t) \end{aligned}\right\} \qquad (9)$$

where x and y are the coordinates of the center of gravity of the model. x is in the direction of flow at the centerline of flow, while y is normal to x and in the plane of the film. Similarly, x_s and y_s are the coordinates of the center of gravity of the sphere. The angle of attack α of the model is found from the relation

$$\alpha = \arctan\left(\frac{y - y_2}{x - x_2}\right)$$

where x_2 and y_2 are the coordinates of any other point on the centerline of the model. All coordinates are taken with respect to some fixed arbitrary reference point in the grid system which appears in each frame of the film.

13. Since the flow of air in the test section is radial, the observed motion of a model will be slightly in error. This is because the x-axis is set parallel to the centerline of flow and the motion of the model is then assumed to be under the influence of a flow that is everywhere parallel. To correct this discrepancy the following procedure is used. In earlier tests it was estimated that a distance X from the diaphragm at the muzzle along the centerline of flow in the test section, the direction of the flow at some point a small distance Y from the centerline is such that the flow appears to have originated at a point on the centerline a distance approximately 0.1 X from the diaphragm. Thus, when a model is at a distance X from the diaphragm and a distance Y from the centerline, the observed motion of the model may be corrected by subtracting the quantity x Y/0.9 X from the y-coordinate of the model. The quantity Y is determined by observing the motion of the sphere. A linear equation of the form $y_s' = {}^{\Delta y_s}/_{\Delta x_s} x_s'$ is fitted by the method of least squares (see Appendix) to the x_s versus y_s data, and the first derivative ${}^{\Delta y_s}/_{\Delta x_s}$ of this equation is found. On the assumption that the sphere travels in the direction of the flow, the distance Y_s from the sphere to the centerline of flow is then taken as $0.9\,{}^{\Delta y_s}/_{\Delta x_s}$ X. Then $Y = Y_s + y - y_s$. As a result of the very small imperfections in its mass distribution and dimensions, the sphere does not travel precisely in the direction of flow. However, the amount that the sphere trajectory deviates from the direction of flow is usually small compared to the angle between the flow direction and the horizontal. In one exception, where $x \geq 193$ inches (the region in which the flow Mach number is greater than 13.5), the magnitude of the flow radiality is less than the probable error introduced when assuming that the sphere travels in the flow direction. Therefore, in this region, no correction is made for flow radiality. For the sake of simplicity, it will henceforth be assumed that the data describing equations (9) have been corrected for flow radiality in the region where this correction is appropriate.

14. The problem remaining is to determine the quantitites C_D, C_L, and C_M as functions of α and Mach number M, by manipulating equations (1) through (4) and the experimental data describing equations (9). Since the first tests were made in the NOL 4-in. Hypersonic Shock Tunnel No. 3, various techniques have been employed to obtain the aerodynamic coefficients. Each method is described in the outline below. Each of Methods I, II, and III is a technique for determining C_D, C_L, and C_M, while Methods

IV and V are techniques used for determining values for C_M only. Methods VI and VII are procedures for calculating the dynamic pressure q.

15. Method I: By dividing each of equations (1) through (3) by equation (4), and manipulating the results, one can obtain the following three relations.

$$C_D = C_{D_S} \frac{A_S m}{A_m m_S} \frac{\ddot{x}}{\ddot{x}_S} \tag{10}$$

$$C_L = C_{D_S} \frac{A_S m}{A_m m_S} \frac{\ddot{y}}{\ddot{x}_S} \tag{11}$$

$$C_M = C_{D_S} \frac{A_S}{A_m} \frac{I}{m_S D_m} \frac{\ddot{\alpha}}{\ddot{x}_S} \tag{12}$$

The quantity C_{D_S} is a fairly well established quantity, and is considered to be equal to 0.88 in the realm of Mach numbers 8 to 15. The other quantitites on the right-hand side of the above three equations are readily measurable, except the ratios of accelerations $\frac{\ddot{x}}{\ddot{x}_S}$, $\frac{\ddot{y}}{\ddot{x}_S}$, and $\frac{\ddot{\alpha}}{\ddot{x}_S}$. These ratios are obtained by first dividing the data of equations (9) into relatively short intervals of time and assuming that over each time interval accelerations are constant. A second-degree equation is then fitted to each set of the data by the method of least squares (see Appendix), and each equation is differentiated twice with respect to time. This second derivative is then taken as a value for the acceleration. For example, an equation of the form $\alpha = C_0 + C_1 t + C_2 t^2$ is fitted to the $\alpha = \alpha(t)$ data, while an equation of the form $X_S = C_{0_S} + C_{1_S} t + C_{2_S} t^2$ is fitted to the $X_S = X_S(t)$ data. These two equations are then differentiated twice, and the ratio of these derivatives, $\frac{C_2}{C_{2_S}}$, is set equal to the ratio of accelerations $\ddot{\alpha}/\ddot{x}_S$. The moment coefficient is then determined through the equation.

$$C_M = C_{D_S} \frac{A_S}{A} \frac{I}{m_S D_m} \frac{C_2}{C_{2_S}}$$

The drag and lift coefficients are also determined in a similar manner. Thus, by this method of analysis, all three aerodynamic coefficients, C_M, C_L, and C_D, of a model, can be determined if the model and the sphere accelerate in a quasi-steady manner. This condition is met when the angle of attack α and dynamic pressure q experience only small changes in a given interval of time.

16. Method II: A double integration of equation (1) yields

$$x - x_1 = \int_0^t \int_0^t \frac{C_D q A_m}{m} dt dt = \frac{A_m}{m} \bar{C}_D \int_0^t \int_0^t q dt dt \qquad (13)$$

where $x = x_1$ and $\frac{dx}{dt} = 0$ when $t = 0$. $\bar{C}_D$ is defined by

$$\bar{C}_D \equiv \frac{\int_0^t \int_0^t C_D q dt dt}{\int_0^t \int_0^t q dt dt} \qquad (14)$$

A similar double integration of equation (4) yields

$$x_s - x_{si} = \int_0^t \int_0^t \frac{C_{D_s} q A_s}{m_s} dt dt = \frac{A_s}{m_s} C_{D_s} \int_0^t \int_0^t q dt dt \qquad (15)$$

where $x_s = x_{si}$ and $\frac{dx_s}{dt} = 0$ when $t = o$. C_{D_s} is assumed to be constant. Dividing equation (13) by equation (14) gives

$$\frac{x - x_i}{x_s - x_{si}} = \frac{A_m}{A_s} \frac{m_s}{m} \frac{\bar{C}_D}{C_{D_s}} \frac{\int_0^t \int_0^t q dt dt}{\int_0^t \int_0^t q dt dt}$$

and finally

$$\bar{C}_D = C_{D_s} \frac{A_s}{A_m} \frac{m}{m_s} \frac{x - x_i}{x_s - x_{si}} \qquad (16)$$

Analogously, if equations (2) and (3) are integrated twice, and each resulting equation divided by equation (15), one will obtain

$$\bar{C}_L = C_{D_s} \frac{A_s}{A_m} \frac{m}{m_s} \frac{y - y_i}{x_s - x_{si}} \qquad (17)$$

$$\bar{C}_M = C_{D_s} \frac{A_s}{A_m} \frac{I}{D_m m_s} \frac{\alpha - \alpha_i}{x_s - x_{si}} \tag{18}$$

where $y=y_i$, $\alpha = \alpha_i$, $\frac{dy}{dt} = 0$, and $\frac{d\alpha}{dt} = 0$ when $t = 0$, and $\bar{C}_L$ and $\bar{C}_M$ are defined by the relations

$$\bar{C}_L \equiv \frac{\int_0^t \int_0^t C_L q \, dt \, dt}{\int_0^t \int_0^t q \, dt \, dt} \tag{19}$$

$$\bar{C}_M \equiv \frac{\int_0^t \int_0^t C_M q \, dt \, dt}{\int_0^t \int_0^t q \, dt \, dt} \tag{20}$$

As α and q approach constant values in the entire time interval zero to t, the values of $\bar{C}_D$, $\bar{C}_L$ and $\bar{C}_M$ approach C_D, C_L and C_M, respectively.

17. Method III: If a model is axisymmetric, its moment and lift coefficients are odd functions of its angle of attack α. Thus,

$$C_M = A\alpha + B\alpha^3 + C\alpha^5 + \cdots$$

$$C_L = A'\alpha + B'\alpha^3 + C'\alpha^5 + \cdots$$

At the same time, the drag coefficient of an axisymmetric model is an even function of α, so that

$$C_D = C_{D_0} + C_{D_1}\alpha^2 + C_{D_2}\alpha^4 + \cdots$$

If α is very small, then one may accurately assume that $C_M = A\alpha$, $C_L = A'\alpha$, and $C_D = C_{D_0}$. For intermediate angles ($-50^\circ < \alpha < 50^\circ$) reasonable approximations are

$$C_M = A\alpha + B\alpha^3 \tag{21}$$

$$C_L = A'\alpha + B'\alpha^3 \tag{22}$$

$$C_D = C_{D_0} + C_{D_1}\alpha^2 \tag{23}$$

Upon substituting equations (21), (22), and (23) into equations (20), (19), and (14), respectively, one obtains

$$\bar{C}_M \int_0^t\int_0^t q\,dt\,dt = A\int_0^t\int_0^t \alpha q\,dt\,dt + B\int_0^t\int_0^t \alpha^3 q\,dt\,dt \tag{24}$$

$$\bar{C}_L \int_0^t\int_0^t q\,dt\,dt = A'\int_0^t\int_0^t \alpha q\,dt\,dt + B'\int_0^t\int_0^t \alpha^3 q\,dt\,dt \tag{25}$$

$$\bar{C}_D \int_0^t\int_0^t q\,dt\,dt = C_{D_0}\int_0^t\int_0^t q\,dt\,dt + C_{D_1}\int_0^t\int_0^t \alpha^2 q\,dt\,dt \tag{26}$$

When the above double integrals are evaluated for two different upper limits, say t_1 and t_2, three sets of two simultaneous equations are obtained. The constants A, B, A', B', C_{D_0}, and C_{D_1} can then be determined, from these simultaneous equations and solutions for the coefficients C_M, C_L and C_D as functions of α will have been found. If the dynamic pressure q can be assumed constant, then q will drop out of equations (24) through (26), and the integrals can be determined by numerically integrating the $\alpha = \alpha(t)$ data. If q is not constant, but quasi-steady, then $q=q(t)$ may be determined by the technique described in Method VI, and the above integrals again found by numerically integrating the appropriate functions of $q(t)$ and $\alpha(t)$.

18. Method IV: As pointed out in Method III, a reasonable assumption for intermediate angles of attack α is that $C_M = A\alpha + B\alpha^3$ Substituting this expression into equation (3) gives

$$(A\alpha + B\alpha^3) q A_m D_m = I\ddot{\alpha}$$

A manipulation of $\ddot{\alpha}$ yields

$$\ddot{\alpha} = \frac{d^2\alpha}{dt^2} = \frac{d}{d\alpha}(\omega^2/2) = \frac{A_m D_m}{I} q(A\alpha + B\alpha^3)$$

where $\omega = \frac{d\alpha}{dt}$.

Now assume q= constant.

$$\int_0^t d\left(\frac{\omega^2}{2}\right) = \frac{A_m D_m}{I} q\left[A\int_{\alpha_i}^{\alpha} \alpha\, d\alpha + B\int_{\alpha_i}^{\alpha} \alpha^3 d\alpha\right]$$

If $\alpha = \alpha_i$ and $\omega = 0$ when t = 0, then

$$\frac{\omega^2}{2} = \frac{A_m D_m}{I} q\left[\frac{1}{2}A\alpha^2 + \frac{1}{4}B\alpha^4\right]_{\alpha_i}^{\alpha}$$

This equation can now be evaluated for two different upper limits, say α_1, and α_2, giving two simultaneous equations from which the constants A and B and hence C_M, can be determined. The resulting expressions for A and B are

$$A = \frac{I}{A_m D_m q} \frac{\omega_1^2(\alpha_2^4 - \alpha_i^4) - \omega_2^2(\alpha_1^4 - \alpha_i^4)}{(\alpha_1^2 - \alpha_i^2)(\alpha_2^4 - \alpha_i^4) - (\alpha_2^2 - \alpha_i^2)(\alpha_1^4 - \alpha_i^4)}$$

$$B = \frac{I}{A_m D_m q} \frac{\omega_2^2(\alpha_1^2 - \alpha_i^2) - \omega_1^2(\alpha_2^2 - \alpha_i^2)}{(\alpha_1^2 - \alpha_i^2)(\alpha_2^4 - \alpha_i^4) - (\alpha_2^2 - \alpha_i^2)(\alpha_1^4 - \alpha_i^4)}$$

The quantitites ω_1, and ω_2 can be determined by fitting a curve to the $\alpha = \alpha(t)$ data using any of various methods, such as the method of least squares, and taking the first derivative of the curve with respect to t. This technique for determing C_M is accurate only if the dynamic pressure q is essentially constant. The dynamic pressure can be determined either by Method VI or Method VII.

19. Method V: According to equation (3),

$$C_M = \frac{I}{qA_mD_m}\frac{d^2\alpha}{dt^2} = \frac{I}{2qA_mD_m}\frac{d}{d\alpha}(\omega^2)$$

Assume q= constant. Then, if $\alpha = \alpha_i$ and $\omega = 0$ when $t = 0$,

$$\int_{\alpha_i}^{\alpha} C_M\, d\alpha = \frac{I}{2qA_mD_m}\int_0^{\omega} d(\omega^2) = \frac{I\omega^2}{2qA_mD_m}$$

Now let $\omega = \omega_o$ when $\alpha = 0$. Then

$$\int_0^{\alpha_i} C_M\, d\alpha = -\frac{I\omega_o^2}{2qA_mD_m}$$

Since two models are used in each shock tunnel test, two values for the term on the right-hand side of the above equation can be obtained from the data extracted from each test, if both test models rotated through zero angle of attack. The quantity ω_o is determined by fitting a curve to the $\alpha = \alpha(t)$ data around the region where $\alpha = 0$ and taking the first derivative of this curve with respect to t. Thus, after several tests are made, several values of the term $-I\omega_o^2/2qA_mD_m$ can be determined. If these values are plotted against the initial angles α_i in each test, then a curve can be fitted to this plot. The first derivative of this curve with respect to α_i will then give C_M as a function of α_i, or angle of attack, since

$$C_M = \frac{d}{d\alpha_i}\left(-\frac{I\omega_o^2}{2qA_mD_m}\right)$$

Again, as in Method IV, the accuracy of the above method of analysis is dependent upon the requirement that the dynamic pressure q be essentially constant.

20. Method VI: By equation (4),

$$q = \frac{m_s\ddot{x}_s}{C_{D_s}A_s}$$

Assume that q is quasi-steady, so that for relatively short intervals of time, q, and hence $\ddot{x}_s$, can be considered constant, then fit equations of the form $x_s = C_{0s} + C_{1s}t + C_{2s}t^2$ to short intervals of the $x_s = x_s(t)$ data by the method of least squares.

If $\ddot{x}_s$ is nearly constant for a given interval of time, the second derivative $\dddot{x}_s$ can be assumed to equal $\ddot{x}_s$, or $\ddot{x}_s = 2C_{2s}$, and the dynamic pressure q in this interval can be accurately estimated.

21. Method VII: Assume q = constant, also assume the velocity V_s of the sphere is zero and $x_s = x_{si}$ when t=0. Then, if equation (4) is integrated twice with respect to t, the resulting equation is

$$q = \frac{2m_s(x_s - x_{si})}{C_{D_s} A_s t^2}$$

and thus, q can be determined directly from the $x_s = x_s(t)$ data.

22. Each of the above methods of analysis when applied to the reduction of experimental data will yield results of varying accuracy and reliability, depending upon the type, quality, and quantity of the data. If for example, $\alpha(t)$ is nearly constant, then Methods I and II will give the most accurate results, whereas, if $\alpha(t)$ varies considerably, then Methods III, IV, and V will give the most accurate results. Method V can be used successfully only if several tests are made. By use of Methods I and II, a single value for C_D, C_L, or C_M is reduced from a given interval of the data, regardless of whether or not the angle of attack varies during this interval. Since C_L and C_M are functions of the angle α, an average value $\overline{\alpha}$ is determined for this interval of data such that

$$\overline{\alpha} = \frac{1}{n}\sum_{i=1}^{n} \alpha_i$$

where $\alpha_i = \alpha(t)$, and n is the number of data points in the given interval. When a single value for either C_L or C_M is determined from an interval of data, the quantity $\overline{\alpha}$ for this same interval is also given. For models that are symmetric in the plane of the film, the drag coefficient C_D is a function of the absolute value of the angle of attack, so that when a single value for C_D is obtained from a given interval of the data the quantity $\overline{|\alpha|}$ for this same interval is also given, where

$$\overline{|\alpha|} = \frac{1}{n}\sum_{i=1}^{n} |\alpha_i|$$

23. A major source of error in the results stems from the difficulty of determining with precision the angle α. Though the variation in α can be observed with accuracy (roughly $\pm$ 0.2°), the value of the angle of attack itself cannot be determined this well. This is due to the effects of the radial flow in the 4-in. Hypersonic Shock Tunnel No. 3. Though the angles of attack are corrected for flow radiality, they are corrected only to the extent of the accuracy to which the degree of radiality is known. The accuracy of the measurement of α is best at the high Mach numbers, since the radiality of the flow is least at these positions. This error in α will introduce greater error in the results, if the results are obtained by numerical integrations of the $\alpha(t)$ data, such as is the case if Method III is used.

24. Ordinarily, for a series of several tests, the scatter of the results can be kept within $\pm$ 5 percent of a mean-value curve (except for the very small values of C_L and C_M such as those that occur at small angles of attack), but if the test models are relatively massive (e.g., greater than 15 grams for a model 3 inches in length), then their accelerations will be small, and the given limit of scatter in the results will be surpassed.

25. It is the opinion of the authors that a model should be tested at least twice at roughly equal conditions. It is felt that the increase in reliability of the results will more than offset the cost of additional tests.

ACKNOWLEDGEMENTS

26. The authors wish to acknowledge the generous assistance and many helpful suggestions of Dr. A. E. Seigel and Mr. V. C. D. Dawson, who were instrumental in the development of this technique. Acknowledgement is also due Mr. R. Piacesi, who was responsible for the programming of the data reduction techniques and Mr. J. B. Watson, who helped develop many of the methods of the analysis.

REFERENCES

(a) Aronson, P. M., Marshall, T., Seigel, A. E., Slawsky, Z. I., and Smiley, E. F., "Shocktube Wind Tunnel Research at the U. S. Naval Ordnance Laboratory," Proceedings of Second Shock Tube Symposium, 5-6 March 1958

(b) Seigel, A. E., and Slawsky, Z. I., "The Use of High Velocity Gun-Like Shocktubes to Obtain Aerodynamic Force Data," 9th Tripartite AXP Research Conference, Vol. III, Canada, April 1959

(c) Seigel, A. E., "Millisecond Measurement of Forces and Moments in Hypersonic Flow," NOL Aeroballistic Research Facilities Dedication and Decennial, NOLR 1238, 25-26 May 1959

(d) Kaegi, E. M., Warren, W. R., Harris, C. J., and Geiger, R. E., "The Capabilities of the Shock Tunnel in the Study of the Aerodynamics of Atmospheric Entry," ARS 15th Annual Meeting, 5-8 December 1960

(e) Noonan, B. J., Waser, R. H., and Dawson, V. C. D., "The NOL 4-in. Hypersonic Shock Tunnel No. 3," NavOrd Report 6787, 17 June 1960

(f) Dawson, V. C. D., "Pressure Gage Design for the Measurement of Pressures in Shocktube Wind Tunnels, Shocktubes, and Guns," NavWeps Report 7326 (In preparation)

(g) Dawson, V. C. D., "Piston Type Strain Gages," NavOrd Report 6251, 13 January 1959

(h) Faymon, K. A., "The Convair Free Jet Hypersonic Shock Tunnel," Report No. ZR-659-018, 2 April 1959

(i) Crapo, B. J., Hill, L. L., and Marshall, T., "A High-Intensity Rectangular--Pulse Light Source for High-Speed Photography," NavOrd Report 6795 (In preparation)

(j) Hill, L. L., "Distortion Problems Encountered in the Model 192 Beckman & Whitley High-Speed Framing Camera," NOLTR 61-10 (In preparation)

(k) Marshall, J. M., "A Pressure Sensitive Detector for Use in Shock Velocity Measurements in Shock Tubes and Tunnels," NOLTR 61-117 (In preparation)

(l) Hilsenrath, J., Beckett, C. W., Benedict, W. S., Fano, L., Hoge, H. J., Masi, J. F., Nuttall, R. L., Touloukian, Y. S., and Woolley, H. W., "Tables of Thermal Properties of Gases," NBS Circular 564, 1 November 1955

(m) Hilsenrath, J., and Beckett, C. W., "Tables of Thermodynamic Properties of Argon-Free Air to 15,000 °K," ARDC Report No. MIPR-AEDC-1, September 1956

APPENDIX

THE METHOD OF LEAST SQUARES

1. Given is a set of data (x_i, t_i) for which $x = x(t)$ and $i=1,2,3,\ldots,n$. It is desired that a curve of the form $x'=C_o+C_1t+C_2t^2$ be fitted through these data in such a way that the sum of the squares of the individual deviations x_i-x' be a minimum, or

$$G=\sum_{i=1}^{n}\left[x_i-(C_o+C_1t_i+C_2t_i^2)\right]^2$$

be a minimum. Now, $G=G(C_o, C_1, C_2)$, so that

$$dG=\frac{\partial G}{\partial C_o}dC_o+\frac{\partial G}{\partial C_1}dC_1+\frac{\partial G}{\partial C_2}dC_2$$

Then the conditions for the fitted curve will be satisfied when

$$\frac{\partial}{\partial C_o}\sum_{i=1}^{n}\left[x_i-(C_o+C_1t_i+C_2t_i^2)\right]^2=0$$

$$\frac{\partial}{\partial C_1}\sum_{i=1}^{n}\left[x_i-(C_o+C_1t_i+C_2t_i^2)\right]^2=0$$

$$\frac{\partial}{\partial C_2}\sum_{i=1}^{n}\left[x_i-(C_o+C_1t_i+C_2t_i^2)\right]^2=0$$

Upon carrying through the above differentiations, we have

$$-2\sum_{i=1}^{n}\left[x_i-(C_o+C_1t_i+C_2t_i^2)\right]=0$$

$$-2\sum_{i=1}^{n}t_i\left[x_i-(C_o+C_1t_i+C_2t_i^2)\right]=0$$

$$-2\sum_{i=1}^{n}t_i^2\left[x_i-(C_o+C_1t_i+C_2t_i^2)\right]=0$$

or

$$\sum_{i=1}^{n} x_i = c_0 n + c_1 \sum_{i=1}^{n} t_i + c_2 \sum_{i=1}^{n} t_i^2$$

$$\sum_{i=1}^{n} x_i t_i = c_0 \sum_{i=1}^{n} t_i + c_1 \sum_{i=1}^{n} t_i^2 + c_2 \sum_{i=1}^{n} t_i^3$$

$$\sum_{i=1}^{n} x_i t_i^2 = c_0 \sum_{i=1}^{n} t_i^2 + c_1 \sum_{i=1}^{n} t_i^3 + c_2 \sum_{i=1}^{n} t_i^4$$

The problem is now one of solving these three simultaneous equations. This is done most simply with the use of determinants.

2. Let

$$D = \begin{vmatrix} n & \sum_{i=1}^{n} t_i & \sum_{i=1}^{n} t_i^2 \\ \sum_{i=1}^{n} t_i & \sum_{i=1}^{n} t_i^2 & \sum_{i=1}^{n} t_i^3 \\ \sum_{i=1}^{n} t_i^2 & \sum_{i=1}^{n} t_i^3 & \sum_{i=1}^{n} t_i^4 \end{vmatrix}$$

$$D_{c_0} = \begin{vmatrix} \sum_{i=1}^{n} x_i & \sum_{i=1}^{n} t_i & \sum_{i=1}^{n} t_i^2 \\ \sum_{i=1}^{n} x_i t_i & \sum_{i=1}^{n} t_i^2 & \sum_{i=1}^{n} t_i^3 \\ \sum_{i=1}^{n} x_i t_i^2 & \sum_{i=1}^{n} t_i^3 & \sum_{i=1}^{n} t_i^4 \end{vmatrix}$$

$$D_{c_1} = \begin{vmatrix} n & \sum_{i=1}^{n} x_i & \sum_{i=1}^{n} t_i^2 \\ \sum_{i=1}^{n} t_i & \sum_{i=1}^{n} x_i t_i & \sum_{i=1}^{n} t_i^3 \\ \sum_{i=1}^{n} t_i^2 & \sum_{i=1}^{n} x_i t_i^2 & \sum_{i=1}^{n} t_i^4 \end{vmatrix}$$

$$D_{C_2} = \begin{vmatrix} n & \sum_{i=1}^{n} t_i & \sum_{i=1}^{n} x_i \\ \sum_{i=1}^{n} t_i & \sum_{i=1}^{n} t_i^2 & \sum_{i=1}^{n} x_i t_i \\ \sum_{i=1}^{n} t_i^2 & \sum_{i=1}^{n} t_i^3 & \sum_{i=1}^{n} x_i t_i^2 \end{vmatrix}$$

Then finally,

$$C_0 = \frac{D_{C_0}}{D}$$

$$C_1 = \frac{D_{C_1}}{D}$$

$$C_2 = \frac{D_{C_2}}{D}$$

3. If it is desired that an equation of the form $x' = C_0 + C_1 t$ be fitted to the same data by the same method, then

$$G = \sum_{i=1}^{n} \left[x_i - (C_0 + C_1 t_i) \right]^2$$

and by the same treatment,

$$C_0 = \frac{\begin{vmatrix} \sum_{i=1}^{n} x_i & \sum_{i=1}^{n} t_i \\ \sum_{i=1}^{n} x_i t_i & \sum_{i=1}^{n} t_i^2 \end{vmatrix}}{\begin{vmatrix} n & \sum_{i=1}^{n} t_i \\ \sum_{i=1}^{n} t_i & \sum_{i=1}^{n} t_i^2 \end{vmatrix}}$$

$$C_1 = \frac{\begin{vmatrix} n & \sum_{i=1}^{n} x_i \\ \sum_{i=1}^{n} t_i & \sum_{i=1}^{n} x_i t_i \end{vmatrix}}{\begin{vmatrix} n & \sum_{i=1}^{n} t_i \\ \sum_{i=1}^{n} t_i & \sum_{i=1}^{n} t_i^2 \end{vmatrix}}$$

4-in. HYPERSONIC SHOCK TUNNEL NO.3

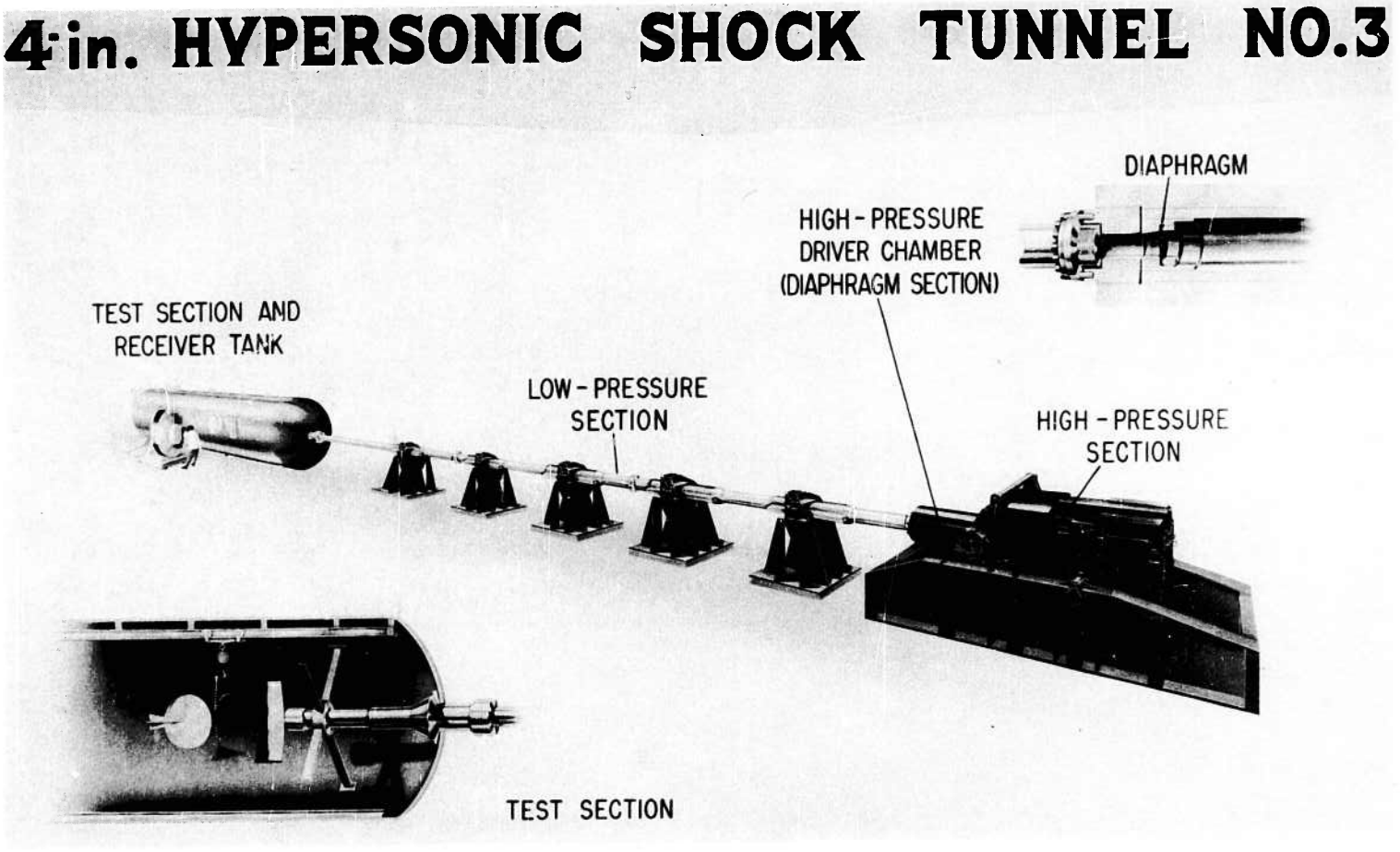

FIG I

NOLTR 61-100

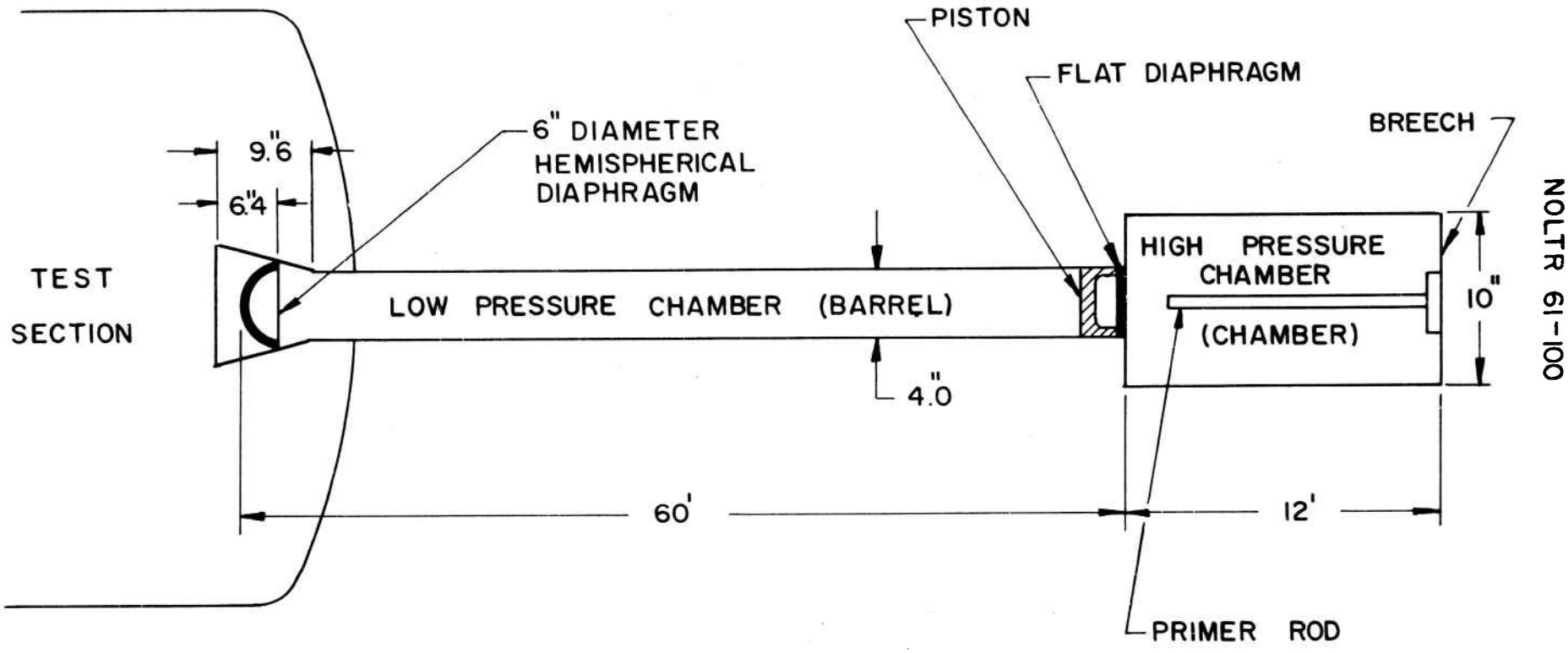

FIG. 2 SCHEMATIC DIAGRAM OF N.O.L. 4 inch HYPERSONIC SHOCK TUNNEL NO. 3

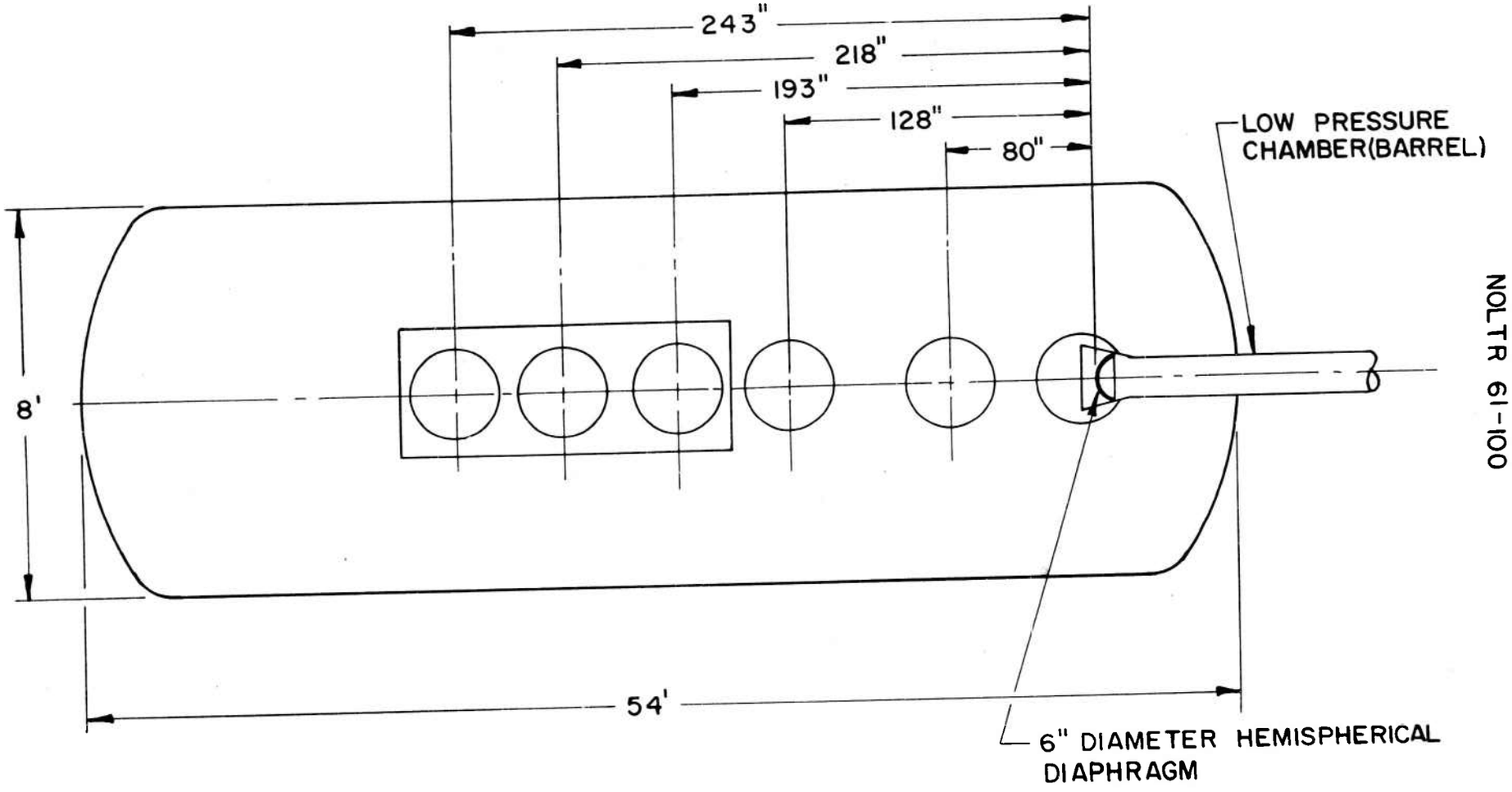

FIG. 3 SCHEMATIC DIAGRAM SHOWING LOCATIONS OF WINDOWS IN RECEIVER TANK OF N.O.L. 4 inch HYPERSONIC SHOCK TUNNEL NO. 3

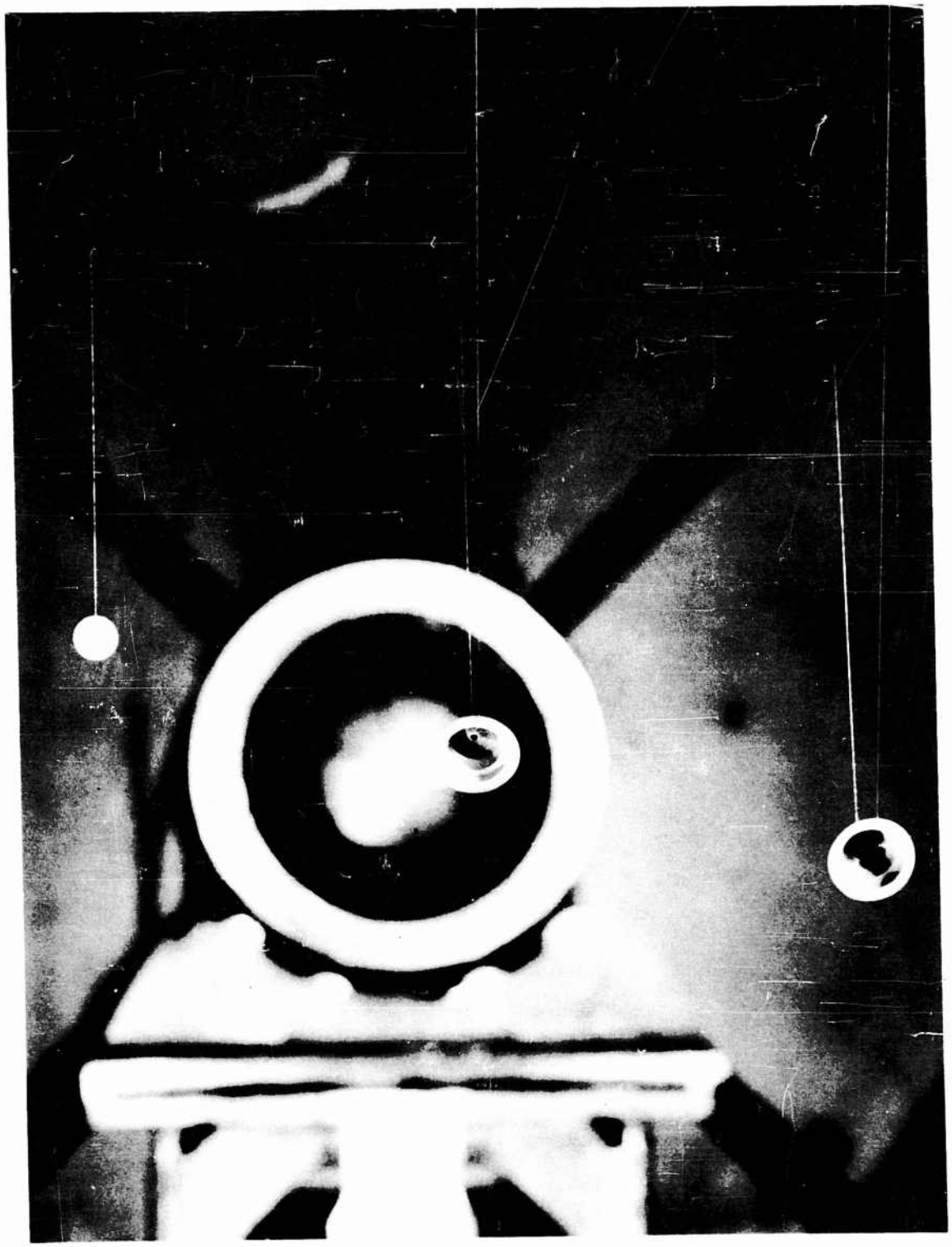

FIG. 4 VIEW OF MODELS FROM INSIDE RECEIVER TANK.

TABLE I

CONDITIONS IN THE NOL 4-IN. HYPERSONIC SHOCK TUNNEL NO. 3

Distance From Muzzle To Models		80 in.	142 in.	218 in.
High-Pressure Chamber	Initial Load	6,000 psi He	6,000 psi He	6,000 psi He
	Powder Charge	30 lbs	30 lbs	30 lbs
	Peak Pressure	30,000 psi	30,000 psi	30,000 psi
Low-Pressure Chamber	Initial Load	450 psi air	450 psi air	350 psi air
	Free-Stream Pressure	9,200 psi	9,200 psi	9,300 psi
	Total Enthalpy	850 Btu/lb	850 Btu/lb	1,080 Btu/lb
	Free-Stream Temperature	1,230°K	1,230°K	1,450°K
	Shockwave Velocity	4,800 ft/sec	4,800 ft/sec	5,400 ft/sec
	Shockwave Mach Number	4.2	4.2	4.7
	Flow Velocity	3,800 ft/sec	3,800 ft/sec	4,400 ft/sec
Expansion Chamber	Flow Mach Number	8	10.9	14.3
	Stagnation Pressure	265 psi	80 psi	25 psi
	Stagnation Temperature	1,800°K	1,800°K	2,200°K
	Free-Stream Pressure	4 psi	0.5 psi	0.1 psi
	Free-Stream Temperature	140°K	80°K	60°K
	Flow Velocity	6,300 ft/sec	6,400 ft/sec	7,300 ft/sec
	Density	0.04 lbs/ft^3	0.009 lbs/ft^3	0.002 lbs/ft^3
	Dynamic Pressure	180 psi	40 psi	12 psi
	Reynolds Number Per Inch	3 x 10^6	10^6	0.5 x 10^6

External Distribution List

	No. of copies
Chief, Bureau of Naval Weapons Department of the Navy Washington 25, D. C.	
Attn: RMMO	1
Attn: RMGA	1
Attn: RRMA	1
Director, Special Projects Department of the Navy Washington 25, D. C.	
Attn: SP-20	4
Attn: SP-27	2
Attn: SP-272	1
Office of Naval Research Room 2709 - T-3 Washington 25, D. C.	
Attn: Head, Mechanics Br.	1
Commanding Officer Office of Naval Research Branch Office, Box 39, Navy 100 Fleet Post Office, New York, N. Y.	5
Director, DTMB Aerodynamics Laboratory Washington 7, D. C.	
Attn: Library	1
Naval Weapons Laboratory Dahlgren, Va.	
Attn: Library	1
Commander U. S. Naval Ordnance Test Station China Lake, Calif.	
Attn: Technical Library	1
Director Naval Research Laboratory Washington 25, D. C.	
Attn: Code 2027	1
Attn: Mr. Edward Chapin, Code 6310	1

	No. of copies
NASA Langley Research Center Langley Field, Va.	
Attn: Librarian	1
Attn: C. H. McLellan	1
Attn: J. J. Stack	1
Attn: Adolf Busemann	1
Attn: Rodger W. Peters (Structures Res. Div.)	1
Attn: Russell Hopko, PARD	1
NASA Ames Research Center Moffett Field, Calif.	
Attn: Librarian	1
NASA Lewis Research Center 21000 Brookpark Rd. Cleveland, Ohio	
Attn: Chief, Propulsion Aerodynamics Div.	1
Attn: Mr. George Mandel, Chief, Library	2
Office of the Assistant Secretary of Defense (R&D) Room 3E1041, The Pentagon Washington 25, D. C.	
Attn: Library (Technical)	1
Research and Development Board Room 3D1041, The Pentagon Washington 25, D. C.	
Attn: Library	2
ASTIA Arlington Hall Station Arlington 12, Va.	
Attn: TIPDR	10
Commander, NMC Point Mugu, Calif.	
Attn: Technical Library	1
Commanding General Aberdeen Proving Ground, Md.	
Attn: Technical Info. Br.	1
Attn: Ballistics Research Laboratories	1

	No. of copies
Director of Intelligence Headquarters, USAF Washington 25, D. C. Attn: AFOIN-3B	1
Commander Wright Air Development Div. Wright-Patterson Air Force Base, Ohio	
Attn: WCOSI-3	2
Attn: WCLSW-5	1
Attn: WCRRD	3
Commander, AFBMD Air Res. & Develop. Command P. O. Box 262 Inglewood, Calif.	
Attn: WDTLAR	1
Attn: WDTVR	2
Chief, DASA The Pentagon Washinton, D. C.	
Attn: Document Library	1
Commanding General Arnold Engineering Development Center Tullahoma, Tenn.	
Attn: Technical Library	1
Attn: AEKS	5
Commanding Officer, DOFL Washington 25, D. C.	
Attn: Library Rm. 211, Bldg. 92	1
NASA George C. Marshall Space Flight Center Huntsville, Alabama	
Attn: M-S&M-PT (Mr. H. A. Connell)	5
Attn: Dr. W. R. Lucas (M-SFM-M)	1
Attn: Dr. Ernst Geissler	1
Office, Chief of Ordnance Department of the Army Washington 25, D. C.	
Attn: ORDTU	1

	No. of copies
APL/JHU 8621 Georgia Ave. Silver Spring, Md.	
Attn: Tech. Reports Group	2
Attn: Dr. D. Fox	1
Attn: Dr. Freeman Hill	1
Attn: Dr. L. L. Cronvich	1
Attn: Librarian	1
AVCO Manufacturing Corp. Research & Advanced Development Div. 201 Lowell Street Wilmington, Mass.	
Attn: Mr. J. P. Wamser	1
AVCO Manufacturing Corp. Everett, Mass.	
Attn: Dr. Kantrowitz	1
General Electric Co. Space Vehicle & Missiles Dept. 21 South 12th St. Philadelphia, Penn.	
Attn: Dr. J. Stewart	1
Attn: Dr. Otto Klima	1
Attn: Mr. E. J. Nolan	1
Attn: Mr. L. McCreight	1
General Electric, Research Lab. 3198 Chestnut St. Philadelphia, Penn.	
Attn: Dr. Leo Steg	1
National Aeronautics and Space Admin. 1520 H Street, N. W. Washington, D. C.	5
NASA High Speed Flight Station Edwards Field, Calif.	
Attn: W. C. Williams	1
Aerospace Corporation El Segundo, Calif.	
Attn: Dr. Bitondo	1

	No. of copies
Lockheed Aircraft Corp. Missiles and Space Div. P. O. Box 504 Sunnyvale, Calif. Attn: Dr. L. H. Wilson	1
Lockheed Aircraft Corp. Research Lab. Palo Alto, California Attn: W. Griffith	1
Atomic Energy Commission Engineering Development Branch Division of Reactor Development Headquarters, US AEC Washington 25, D. C.	
Attn: Mr. J. M. Simmons	1
Attn: Mr. M. J. Whitman	1
Attn: Mr. J. Conners	1
University of California Lawrence Radiation Laboratory P. O. Box 808 Livermore, Calif.	
Attn: Mr. W. M. Wells, Propulsion Div.	1
Attn: Mr. Carl Kline	1
Oak Ridge National Laboratory P. O. Box E Oak Ridge, Tenn. Attn: Mr. W. D. Manly	1
Polytechnic Institute of Brooklyn 527 Atlantic Avenue Freeport, N. Y. Attn: Dr. Paul A. Libby	1
General Applied Sciences Laboratories, Inc. Merrick and Stewart Avenues East Meadow, New York Attn: Mr. Robert Byrne	1
Jet Propulsion Laboratory 4800 Oak Grove Drive Pasadena 3, Calif.	
Attn: I. R. Kowlan, Chief, Reports Group	1
Attn: Dr. L. Jaffee	2

	No. of copies
Los Alamos Scientific Laboratory P. O. Box 1663 Los Alamos, New Mexico Attn: Dr. Donald F. MacMillan (N-1 Group Leader)	1
Institute for Defense Analyses Advanced Research Projects Agency Washington 25, D. C. Attn: Mr. W. G. May General Sciences Branch	1
Kaman Aircraft Corporation Nuclear Division Colorado Springs, Colorado Attn: Dr. A. P. Bridges	1
U. S. Atomic Energy Commission P. O. Box 62 Oak Ridge, Tennessee Attn: TRI:NLP:ATD:10-7	1
Sandia Corporation Livermore Laboratory P. O. Box 969 Livermore, Calif.	1
United Aircraft Corporation Research Laboratories East Hartford 8, Conn. Attn: Mr. H. J. Charette	1
Attn: Mr. H. Taylor	1
Sandia Corporation Sandia Base Albuquerque, N. Mexico Attn: Mr. Alan Pope	1
Defense Metals Information Center Battelle Memorial Institute 505 King Avenue Columbus 1, Ohio	1
Commanding General Army Rocket and Guided Missile Agency Redstone Arsenal, Alabama Attn: John Morrow	1

	No. of copies
National Bureau of Standards Washington 25, D. C. Attn: Dr. Galen B. Schubauer	1
Cornell Aeronautical Laboratory 4455 Genesee Street Buffalo, N. Y. Attn: Dr. Gordon Hall	1
Rand Corporation 1700 Main St. Santa Monica, Calif. Attn: J. L. Raymond	1

Naval Ordnance Laboratory, White Oak, Md.
(NOL technical report 61-100)
THE MEASUREMENT OF AERODYNAMIC FORCES AND MOMENTS IN THE NOL 4-IN. HYPERSONIC SHOCK TUNNEL NO. 3 (U), by D.F. Gates and D.N. Bixler. 7 Sept. 1961. 24p. illus., table. (Ballistics research report 51).
UNCLASSIFIED

Light-weight models of missiles are suspended by fine threads in the shock tunnel test section. These models, along with a similarly suspended sphere, break free from their supporting threads and experience free flight at flow initiation. Motion of the models and sphere is recorded photographically with a high-speed framing camera and coordinates are read from the resulting film strips. Methods of analysis are discussed for determining aerodynamic force and moment coefficients from resulting data.

1. Shock tubes - Design
2. Shock tubes - Flow
3. Missiles - Aerodynamics
4. Missiles - Shock tube tests
5. Aerodynamics - Measurements
I. Title
II. Gates, David F.
III. Bixler, David N., jt. author
IV. Series

Naval Ordnance Laboratory, White Oak, Md.
(NOL technical report 61-100)
THE MEASUREMENT OF AERODYNAMIC FORCES AND MOMENTS IN THE NOL 4-IN. HYPERSONIC SHOCK TUNNEL NO. 3 (U), by D.F. Gates and D.N. Bixler. 7 Sept. 1961. 24p. illus., table. (Ballistics research report 51).
UNCLASSIFIED

Light-weight models of missiles are suspended by fine threads in the shock tunnel test section. These models, along with a similarly suspended sphere, break free from their supporting threads and experience free flight at flow initiation. Motion of the models and sphere is recorded photographically with a high-speed framing camera and coordinates are read from the resulting film strips. Methods of analysis are discussed for determining aerodynamic force and moment coefficients from resulting data.

1. Shock tubes - Design
2. Shock tubes - Flow
3. Missiles - Aerodynamics
4. Missiles - Shock tube tests
5. Aerodynamics - Measurements
I. Title
II. Gates, David F.
III. Bixler, David N., jt. author
IV. Series

Naval Ordnance Laboratory, White Oak, Md.
(NOL technical report 61-100)
THE MEASUREMENT OF AERODYNAMIC FORCES AND MOMENTS IN THE NOL 4-IN. HYPERSONIC SHOCK TUNNEL NO. 3 (U), by D.F. Gates and D.N. Bixler. 7 Sept. 1961. 24p. illus., table. (Ballistics research report 51).
UNCLASSIFIED

Light-weight models of missiles are suspended by fine threads in the shock tunnel test section. These models, along with a similarly suspended sphere, break free from their supporting threads and experience free flight at flow initiation. Motion of the models and sphere is recorded photographically with a high-speed framing camera and coordinates are read from the resulting film strips. Methods of analysis are discussed for determining aerodynamic force and moment coefficients from resulting data.

1. Shock tubes - Design
2. Shock tubes - Flow
3. Missiles - Aerodynamics
4. Missiles - Shock tube tests
5. Aerodynamics - Measurements
I. Title
II. Gates, David F.
III. Bixler, David N., jt. author
IV. Series

Naval Ordnance Laboratory, White Oak, Md.
(NOL technical report 61-100)
THE MEASUREMENT OF AERODYNAMIC FORCES AND MOMENTS IN THE NOL 4-IN. HYPERSONIC SHOCK TUNNEL NO. 3 (U), by D.F. Gates and D.N. Bixler. 7 Sept. 1961. 24p. illus., table. (Ballistics research report 51).
UNCLASSIFIED

Light-weight models of missiles are suspended by fine threads in the shock tunnel test section. These models, along with a similarly suspended sphere, break free from their supporting threads and experience free flight at flow initiation. Motion of the models and sphere is recorded photographically with a high-speed framing camera and coordinates are read from the resulting film strips. Methods of analysis are discussed for determining aerodynamic force and moment coefficients from resulting data.

1. Shock tubes - Design
2. Shock tubes - Flow
3. Missiles - Aerodynamics
4. Missiles - Shock tube tests
5. Aerodynamics - Measurements
I. Title
II. Gates, David F.
III. Bixler, David N., jt. author
IV. Series

Naval Ordnance Laboratory, White Oak, Md.
(NOL technical report 61-100)
THE MEASUREMENT OF AERODYNAMIC FORCES AND MOMENTS IN THE NOL 4-IN. HYPERSONIC SHOCK TUNNEL NO. 3 (U), by D.F. Gates and D.N. Bixler. 7 Sept. 1961. 24p. illus., table. (Ballistics research report 51).
UNCLASSIFIED

Light-weight models of missiles are suspended by fine threads in the shock tunnel test section. These models, along with a similarly suspended sphere, break free from their supporting threads and experience free flight at flow initiation. Motion of the models and sphere is recorded photographically with a high-speed framing camera and coordinates are read from the resulting film strips. Methods of analysis are discussed for determining aerodynamic force and moment coefficients from resulting data.

1. Shock tubes - Design
2. Shock tubes - Flow
3. Missiles - Aerodynamics
4. Missiles - Shock tube tests
5. Aerodynamics - Measurements
I. Title
II. Gates, David F.
III. Bixler, David N., jt. author
IV. Series

Naval Ordnance Laboratory, White Oak, Md.
(NOL technical report 61-100)
THE MEASUREMENT OF AERODYNAMIC FORCES AND MOMENTS IN THE NOL 4-IN. HYPERSONIC SHOCK TUNNEL NO. 3 (U), by D.F. Gates and D.N. Bixler. 7 Sept. 1961. 24p. illus., table. (Ballistics research report 51).
UNCLASSIFIED

Light-weight models of missiles are suspended by fine threads in the shock tunnel test section. These models, along with a similarly suspended sphere, break free from their supporting threads and experience free flight at flow initiation. Motion of the models and sphere is recorded photographically with a high-speed framing camera and coordinates are read from the resulting film strips. Methods of analysis are discussed for determining aerodynamic force and moment coefficients from resulting data.

1. Shock tubes - Design
2. Shock tubes - Flow
3. Missiles - Aerodynamics
4. Missiles - Shock tube tests
5. Aerodynamics - Measurements
I. Title
II. Gates, David F.
III. Bixler, David N., jt. author
IV. Series

Naval Ordnance Laboratory, White Oak, Md.
(NOL technical report 61-100)
THE MEASUREMENT OF AERODYNAMIC FORCES AND MOMENTS IN THE NOL 4-IN. HYPERSONIC SHOCK TUNNEL NO. 3 (U), by D.F. Gates and D.N. Bixler. 7 Sept. 1961. 24p. illus., table. (Ballistics research report 51).
UNCLASSIFIED

Light-weight models of missiles are suspended by fine threads in the shock tunnel test section. These models, along with a similarly suspended sphere, break free from their supporting threads and experience free flight at flow initiation. Motion of the models and sphere is recorded photographically with a high-speed framing camera and coordinates are read from the resulting film strips. Methods of analysis are discussed for determining aerodynamic force and moment coefficients from resulting data.

1. Shock tubes - Design
2. Shock tubes - Flow
3. Missiles - Aerodynamics
4. Missiles - Shock tube tests
5. Aerodynamics - Measurements
I. Title
II. Gates, David F.
III. Bixler, David N., jt. author
IV. Series

Naval Ordnance Laboratory, White Oak, Md.
(NOL technical report 61-100)
THE MEASUREMENT OF AERODYNAMIC FORCES AND MOMENTS IN THE NOL 4-IN. HYPERSONIC SHOCK TUNNEL NO. 3 (U), by D.F. Gates and D.N. Bixler. 7 Sept. 1961. 24p. illus., table. (Ballistics research report 51).
UNCLASSIFIED

Light-weight models of missiles are suspended by fine threads in the shock tunnel test section. These models, along with a similarly suspended sphere, break free from their supporting threads and experience free flight at flow initiation. Motion of the models and sphere is recorded photographically with a high-speed framing camera and coordinates are read from the resulting film strips. Methods of analysis are discussed for determining aerodynamic force and moment coefficients from resulting data.

1. Shock tubes - Design
2. Shock tubes - Flow
3. Missiles - Aerodynamics
4. Missiles - Shock tube tests
5. Aerodynamics - Measurements
I. Title
II. Gates, David F.
III. Bixler, David N., jt. author
IV. Series